Materials Science Forum
ISSN: 1662-9752, Vol. 1185, pp 99-109
doi:10.4028/p-61pDv7

Submitted: 2026-01-19
Revised: 2026-02-13
Accepted: 2026-02-24
Online: 2026-04-15

Effect of Fiber Length in Friction Stir Welding of Discontinuous Composites

Clark Austin[1,4,a], Barnett Philip[2,b], Mamros Elizabeth[3,c], Young Brian[4,d] and Ragai Ihab[4,e*]

[1]GROB Systems Inc., Bluffton, OH 45817, USA

[2]University of Tennessee, Knoxville, TN 37996, USA

[3]Bucknell University, Lewisburg, PA 17837, USA

[4]The Pennsylvania State University, Erie, PA 16563, USA

[a]aclark@grobsystems.com, [b]pbarnet3@utk.edu, [c]elizabeth.mamros@bucknell.edu, [d]bay101@psu.edu, [e*]ihab.ragai@psu.edu

*corresponding author

Keywords: FSW, carbon fiber reinforced polymers, polyphenylene sulfide, microstructure.

Abstract. Friction stir welding (FSW) is widely used to bond metals and polymers to create large structures from standardized geometric components. However, FSW has found more limited use in traditional continuous fiber reinforced composites due to the risk of damage to the reinforcing fibers, including fiber misorientation and fragmentation. The process is more amenable to discontinuous fiber composites, which often take the form of injection molding compounds reinforced with short, milled fibers, for which the mechanical performance is significantly degraded. An emerging class of materials, recycled carbon fiber nonwovens, contain long discontinuous fibers that imbue their composites with mechanical performance that bridges the gap between injection molding compounds and continuous fiber laminates, while also decreasing the energy footprint of the materials. This work evaluates this class of materials, alongside injection molding compounds, to develop new insights into the bonding of composite structures using friction stir welding. The bridging effect of discontinuous fibers across the bondline is evaluated using optical microscopy to link processing conditions and fiber length to the resulting performance. Fiber migration was observed in the weld area, though mechanical interlocking was the primary mechanism of bonding in the weld zone. While samples failed at a fraction of the neat materials nominal strength, increased fiber length was found to have a beneficial effect on the apparent tensile and lap shear strength on welds in this study. The new insights gained represent an important step towards the adoption of the FSW process as a means of rapidly manufacturing large composite structures made of carbon fiber/PPS or other fiber-reinforced polymers to enable deployable structures from standardized geometric components.

Introduction

Fiber-Reinforced Polymers.

In polymers with fiber reinforcement, the bridging effect is observed when fibers cross from one face of a delamination to the other, beneficially increasing the strength of the polymer [1]. Both fiber length and orientation have been found to play a role in the strength of reinforced polymers [2]. In particular, fiber length plays a major role in the strength of composites, with fibers below the critical shear transfer length failing due to transfer stress from the matrix to fiber. Below this critical length, fiber pull-out is the dominant failure mechanism, while above this length, fiber fracture dominates. For an ideal composite with mono-strength fibers and perfect dispersion, the strength will theoretically be independent of fiber length beyond the critical fiber length, but such materials do not exist in practice. Instead, real composite materials exhibit a distribution of fiber lengths and fiber strengths, as well as inhomogeneous dispersion leading to stress concentrations that reduce strength. For example, in recent work by Barnett et al., carbon fiber reinforced polyphenylene sulfide (CF/PPS)

composite tensile strength and modulus were shown to exhibit strong fiber length dependence [3]. For injection molding (IM) compounds, they demonstrated that doubling the fiber length resulted in a 28% increase in tensile strength despite a substantial reduction in total achieved fiber volume fraction (36% for the shorter fibers and 12% for the longer).

Increasing the fiber length far beyond the critical fiber length yields much higher performance at similar fiber volume fractions, as shown in Table 1. Recent efforts have focused on the development of long discontinuous fiber composites that offer greater formability for complex geometries than continuous fiber laminates while retaining moderate performance that exceeds IM compounds. Examples include platelet composites [4] and quasi-isotropic nonwovens [5], which offer unique manufacturing and performance benefits, making them well positioned for low-cost, high-volume production. Compared to platelet composites, which use precisely chopped virgin fiber prepreg, nonwovens are amenable to a range of fiber lengths and feedstocks, including recycled fiber, and achieve similar tensile strength at a significantly reduced fiber volume fraction, further reducing cost.

Table 1. Performance of common CF/PPS composite formats.

Material	Format	Fiber Volume Fraction [%]	Tensile Modulus [GPa]	Tensile Strength [MPa]
Toray Cetex TC1100 [6]	Woven Fabric	50	58	752
Mitsubishi Techtron PSBG PPS [7]	Injection Molding Compound	38	6.3	35
Toray Cetex MC1100 [8]	Platelet Molding Compound	59	41.4	207
Carded Organosheets [5]	Nonwoven	29	25	204

Friction Stir Welding.

When joining materials by FSW, the coefficient of friction (CoF) of the workpieces must be considered, as the heat generated between the workpiece and the rotating tool shoulder is the primary source of heat input for the weld [9]. The heat generated from the rotation of the tool shoulder, by way of sliding and sticking forces, softens the workpiece material allowing for plastic deformation along the rotational path of the tool [10]. The CoF of CF/PPS is typically lower than neat PPS [11], which reduces the thermal effect from the rotating tool shoulder. Especially in thermoplastics, the CoF and thermal conductivity are lower than metals, which drives the requirement for pre-heating in order to reach temperatures suitable for plastic deformation [12][13]. It is for these reasons that parameter selection and pre-heating are critical factors in creating a sound weld in CF/PPS. When FSW polymers, the weld bond relies on diffusion across the polymer-polymer interface in intimate contact above the glass transition temperature, T_g [14]. The reptation time of the polymer, an inversely related function of temperature, must be reached to achieve complete bonding across the interface. In CF reinforced polymers, fiber characteristics such as length, orientation, and fiber volume fraction are also very influential on joint strength [15]. It is noted that welded CF polymers often exhibit lower strength than their virgin counterparts due to disruption and a transverse flow of fibers in relation to the seam. However, if fibers adequately span the weld line and sufficient polymer diffusion occurs, the strength of CF reinforced welds should improve.

The work presented herein evaluates the feasibility of bonding composite structures using FSW. The findings from this study will be used to further develop joining practices of CF/PPS for use in larger composite structures than can be made by molding processes. Limitations on mold size and a knowledge gap in joining CF/PPS by FSW, especially that of the recycled nonwoven discontinuous type, hinders the ability for the manufacturing of large robust structures and components. By developing a feasible and practical method for joining CF/PPS by FSW, larger lightweight components can be assembled at lower cost for use in fields, such as aerospace and defense, where strength-to-weight ratios prove critical.

Materials and Methodology

Materials.

To fully understand the relationship between fiber length and bridging at the bondline, multiple PPS formats were tested in similar and dissimilar lap joints. Injection molding was used to manufacture CF/PPS (Electrafil PPS CF50 3DP, TechmerPM) plates containing milled CF ~135μm in length (herein referred to as IM) along with neat PPS plates (Fortron 0203, Celanese). Square plaques (152.4 mm × 152.4 mm) were molded in an Arburg 570A 2000-800. The front barrel temperatures were set to 316 °C. The mold was maintained at 150 °C with the use of a Regloplas P160M steam temperature controller. A fill rate of 100 cc/sec was used to fill the cavity. The natural PPS required 14.12 MPa and the carbon fiber filled PPS required 118.84 MPa to fill the cavity 95% full. Prior to molding the material, the pellets were dried at 65°C for a minimum of 8 hours. The plaques were molded at a 44-second cycle.

Additionally, compression molding was used to manufacture CF/PPS plates from recycled "short" chopped carbon fiber nonwovens (Gen 2 Carbon) with lengths of ~38.8 ± 22.2 mm (herein referred to as CMS). Continuous unidirectional carbon fiber prepregs (P20053-12X, Teijin Carbon) were used to manufacture quasi-isotropic laminates (herein referred to as CML). Compression molding was done at 300 °C for 5 minutes and then cooled under 3 MPa pressure for the recycled fiber nonwovens and following the manufacturer's recommended cycle for the prepregs. Materials tested along with experimental joints are shown in Table 2.

Table 2. Samples used in experiments.

Sample #	Top Plate	Bottom Plate
1	IM	IM
2	IM	CMS
3	IM	CML
4	CMS	CMS
5	CMS	IM
6	CML	CML
7	CMS	Neat

Tensile Testing.

Tensile testing of the CML material was completed in accordance with ASTM D3039M standard using straight-sided specimens [16]. The strain was measured using 2-D digital image correlation (VIC 2D, Correlated Solutions). The tensile properties of the CMS materials were acquired as part of previous work [5]. The goal of this test was to evaluate the baseline performance of the different materials for comparison. Additionally, tensile testing samples were machined out the IM plaques in accordance with ASTM D638 [17]. The tests were conducted using an Instron Universal Testing Machine with a 30 kN load cell. The tests were run at 1.0 mm/min until failure. Strain was calculated using the crosshead displacement. Three samples per plaque per material were tested.

IZOD Impact Testing.

The impact performance was completed according to the ASTM D256 standard [19]. The goal of this test was to elucidate the effect of fiber length on the impact performance as a means of quantifying fiber bridging within each material. An impact energy of 11.3 J was used to test the CMS and CML samples (IT503, Tinius Olsen). An impact-type hammer with a pendulum weight of 1.0 kg [2.2 lb] and energy at impact of 6.1 J [4.5 ft-lb] was utilized for IM samples. Results are reported in terms of energy absorbed per unit of specimen cross-sectional area under the notch. Three samples from each IM material were tested.

Friction Stir Welding.

A lap joint configuration was used for all tests. Parameters used for FSW were a feed rate of 5 mm/min, tool rotation speed of 1500 rpm in a counterclockwise direction, a shoulder plunge depth 1

mm below material surface and a 5-second dwell before welding. All welding was performed in a horizontal 3-axis CNC machine. A weld length of 100 mm was utilized for all samples. The FSW tool used had a pin length of 5 mm, pin diameter of 6 mm, shoulder diameter of 20 mm and a threaded triangular truncated fluted pin profile. All plates were 3.175 mm in thickness, creating a weld stack up of 6.35 mm; thus, giving 95% pin penetration in the weld. A schematic of the pin depth in the workpieces and diagram of the FSW tool is shown in Fig. 1. A Creality Ender-3 S1 3D printer was modified for use as a preheating unit to achieve 85 °C in the samples before welding. Preheating was accomplished on the bottom sample via the print bed under an aluminum plate while the top sample utilized the heating element intended for the printer nozzle. A steel bar was clamped between the top sample and nozzle heating element to aid in thermal distribution. An image of the experimental setup is shown in Fig. 2. Both heating elements were set to 100 °C and monitored until the material reached 85 °C. An Optris 640i LT infrared (IR) camera with a wavelength range of 8-14 µm was used to monitor and collect the temperature distribution during welding as shown in Fig. 3. Emissivity was set to 1.0 for all samples as the top material surface was black in color. An unobstructed line of sight between the IR camera and workpieces was set to 1 m. Tool occlusion was noted as a factor in the experimental setup. The maximum measured temperatures were likely lower than the actual temperature under the tool during welding. While this is a limitation of IR measurement, trends in the measured temperature values among samples were compared equivalently. An AMTI MC12-6-4000 transducer was used to collect force readings in X, Y, and Z directions during welding.

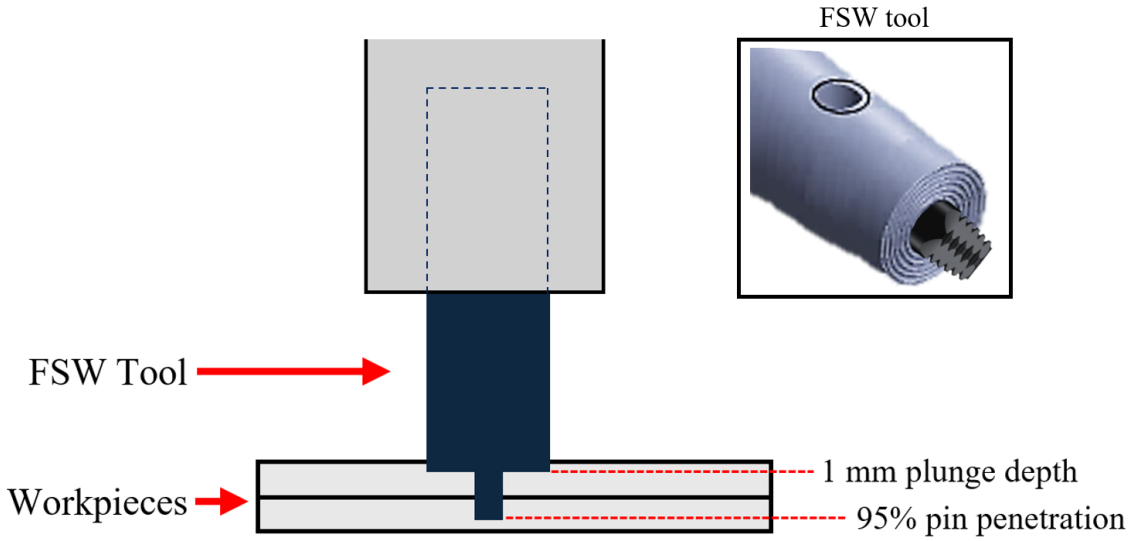

Fig. 1. FSW tool pin depth diagram.

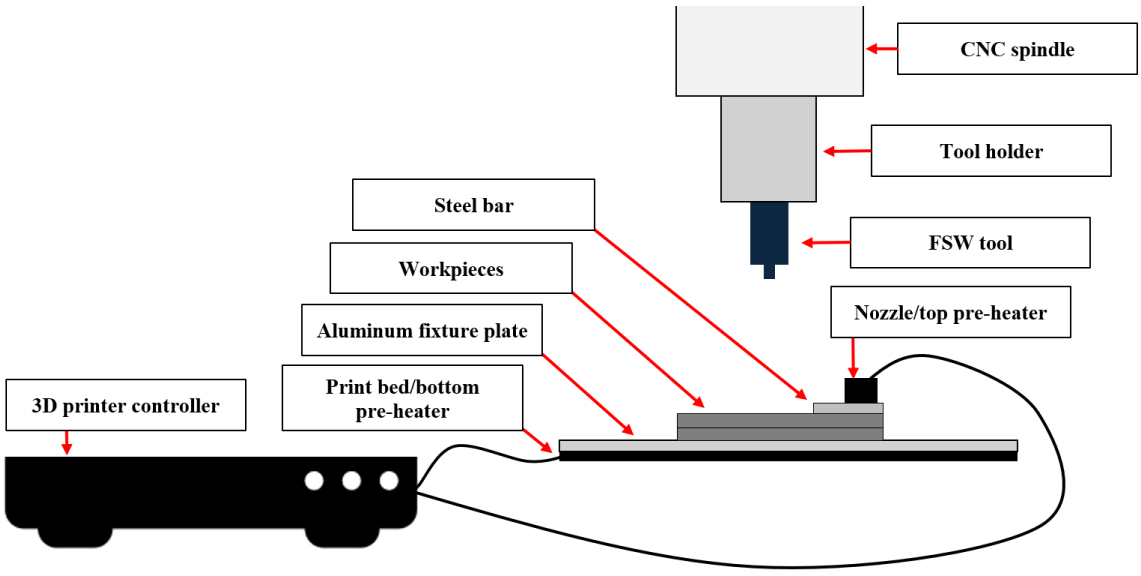

Fig. 2. Schematic of experimental setup.

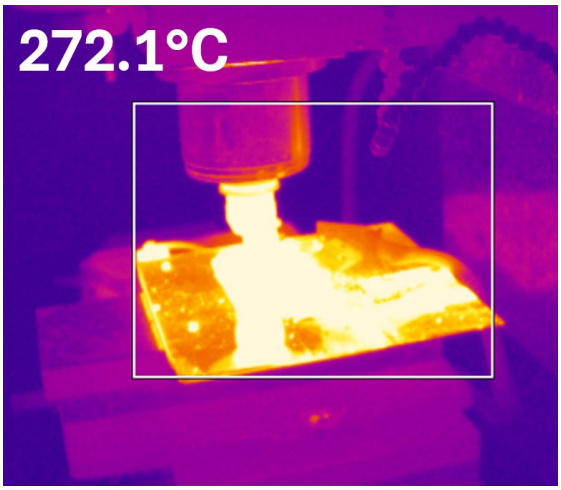

Fig. 3. Thermal image during welding of sample 6 with maximum temperature value recorded at that instant.

Lap Shear Testing.

Lap shear testing of welded specimens was completed according to the ASTM D5868 standard [18] using specimens with a modified geometry (nominally 76 mm total length with 25 mm × 25 mm overlap) and G-10 fiberglass doublers. The samples were gripped 20 mm from each end and loaded at a rate of 13 mm/min. A minimum of three specimens were tested for each sample type with the exception of sample 1 for which only a single specimen was available.

Optical Microscopy.

Optical microscopy was used to evaluate the surface roughness and microstructures of the composites (VHX-7000, Keyence). The surface roughness of the weld area was analyzed using the optical profilometry feature of the microscope to report the arithmetical mean height (S_a), the maximum height (S_z), and the root mean square height (S_q). A minimum of four surfaces were measured for each sample type. Samples were also extracted from the end of the weld region, mounted in epoxy, and polished to observe the weld microstructure. The weld area size in the base material was measured using the open-source Fiji image analysis software [20]. The weld area size was measured for one specimen per sample type.

Differential Scanning Calorimetry (DSC).

Differential scanning calorimetry was used to study the crystallization and melting behavior of the composites. Samples of 4 to 7 mg mass were heated from 20 to 350 °C in a nitrogen atmosphere at 20 °C per minute using a Perkin Elmer DSC 8500. The samples underwent two heating cycles. The enthalpy of melting was taken from the first heating cycle to identify the crystalline percentage using equation (1):

$$X_c = \frac{\Delta H_m}{\Delta H_f\left(1 - W_f\right)} \tag{1}$$

where ΔH_m is the measured melting enthalpy, ΔH_f is the heat of fusion of PPS taken as 88.37 J/g, and W_f is the weight fraction of fiber in the sample. The melting onset and peak temperatures were identified from the second heating ramp, which provides more consistent data due to enhanced thermal contact but loses information pertaining to the thermal history of the as-processed material. A minimum of three samples each were extracted from within the weld zone and on the edges furthest from the weld zone. The goal of this test was to identify if the FSW process led to changes in the thermal properties that might indicate material degradation due to heat and shearing in the weld zone.

Results and Discussion

Baseline Properties.

The tensile and IZOD impact properties of the baseline materials are provided in Table 3. As anticipated, the highest performing material was the CML, whose continuous fibers more effectively translate loads across the composites. The modulus of the quasi-isotropic CML laminates was quite similar to that of the CMS, due to the mildly anisotropic nature of the nonwovens (anisotropy ratio of roughly 2:1 [5], yielding a quasi-isotropic laminate modulus of approximately 25 GPa). The strength of the continuous fiber laminates was much improved, largely attributed to the reduced stress concentrations that cause premature failure in discontinuous fiber composites (as evident from the reduced failure strain). Still, for stiffness-driven applications, CMS laminates may be desirable, especially in cases such as thin skins bonded to CML stiffeners.

For the IM samples, tensile results are also shown in Table 3. The addition of carbon fibers to the PPS matrix reduced the elongation and ultimate strength. This could be attributed to the increased stiffness and brittleness of the material. Additionally, the decline could also be attributed to stress concentration at the ends of the fibers and agglomeration within the matrix. The IZOD results indicate that milled carbon fibers enhance the toughness of PPS. This could be attributed to the carbon fibers acting as obstacles to the propagation of cracks within the PPS matrix. When a crack reaches a fiber, it gets deflected along the fiber-matrix interface and causes the fiber to debond or causes the fiber to break. Each of these scenarios consumes a notable amount of energy, thereby increasing its overall toughness, even while becoming more brittle in a simple tensile test.

Table 3. Mechanical Performance Results for PPS.

Material	Fiber Volume Fraction [%]	Tensile Strength [MPa]	Tensile Modulus [GPa]	Failure Strain [%]	IZOD Impact Resistance [kJ/m^2]
Neat	0	62.4 ± 10.0	2.3 ± 0.1	3.19 ± 0.62	1.55 ± 0.3
IM	36	49.7 ± 2.1	6.2 ± 0.9	0.98 ± 0.22	3.11 ± 0.4
CMS	32	268 ± 32.3	34 ± 2.6	0.80 ± 0.09	15.3 ± 1.0
CML	53	594.8 ± 7.1	38.8 ± 0.9	1.61 ± 0.07	99.4 ± 7.9

Thermomechanical Analysis.

Thermal and longitudinal force measurements were collected for all samples during welding. Maximum temperature values are shown in Table 4. Force data in the longitudinal direction, that is in the direction of the weld seam, is shown in Table 5. Force values are partitioned by first quartile value (Q1), median, third quartile value (Q3) and maximum along with standard deviation. In general, when IM samples were welded in the top plate position (samples 1-3), lower temperatures were generated than with CM samples in the top plate position (samples 4-7). This can be attributed to lower frictional forces as shorter fibers slide past each other in the weld zone. The decrease in temperature for sample 7 (CMS/Neat) is attributed to reduced friction in the neat PPS portion of the weld zone. In general, higher variation in the weld force was observed for samples containing injection molded portions (samples 1-3, 5, and 7). The lowest variation in weld force was for sample 6, which also contains the most homogenous microstructure. The cause of these variations may be changes in material flow that vary spatially alongside variable microstructure.

Table 4. Temperature data (°C).

Sample	Maximum
1	214.9
2	229.9
3	215.2
4	275.0
5	275.0
6	275.0
7	260.3

Table 5. Longitudinal force data (N).

Sample	Q1	Median	Q3	Maximum	Mean	Std Dev (σ)
1	18.9	46.7	75.3	134.2	48.6	33.2
2	25.2	49.7	77.2	133.5	51.8	31.1
3	39.6	64.8	91.6	143.6	63.2	36.9
4	45.0	70.9	102.7	130.0	69.5	38.2
5	60.6	92.3	130.1	160.8	89.1	43.4
6	54.6	72.5	89.4	106.7	67.2	28.4
7	13.4	37.6	70.5	113.6	42.2	32.6

Lap Shear Testing.

All welded samples failed in invalid failure modes – rather than failing in shear at the lap joint, the failure was in tension at the weakest side of the welded structure. In most cases, this was the weld side (samples 2, 3, 4, and 6); however, when a strong material was welded to a weaker base material (samples 5 and 7) the failure transitioned to the base side. Sample 1 was an exception to this result, failing instead by pull-out of the welded region and separation into the two original pieces, indicating that the milled carbon fiber was too short to effectively bridge the weld interface. The three failure modes are shown in Fig. 4. The observed behavior was consistent for all specimens within a sample set. In all cases, the weld appeared to be less of an adhesive bond and more of a mechanical interlocking mechanism. As such, the apparent tensile and shear strengths have been reported based on the failure side thickness and width and the overlap area, respectively. Apparent tensile and lap shear strength are graphed in Fig. 5. These bar graphs show the mean strength and standard deviation for each sample type. The mechanical strength of the welds in this study was far below the strength of the unwelded materials.

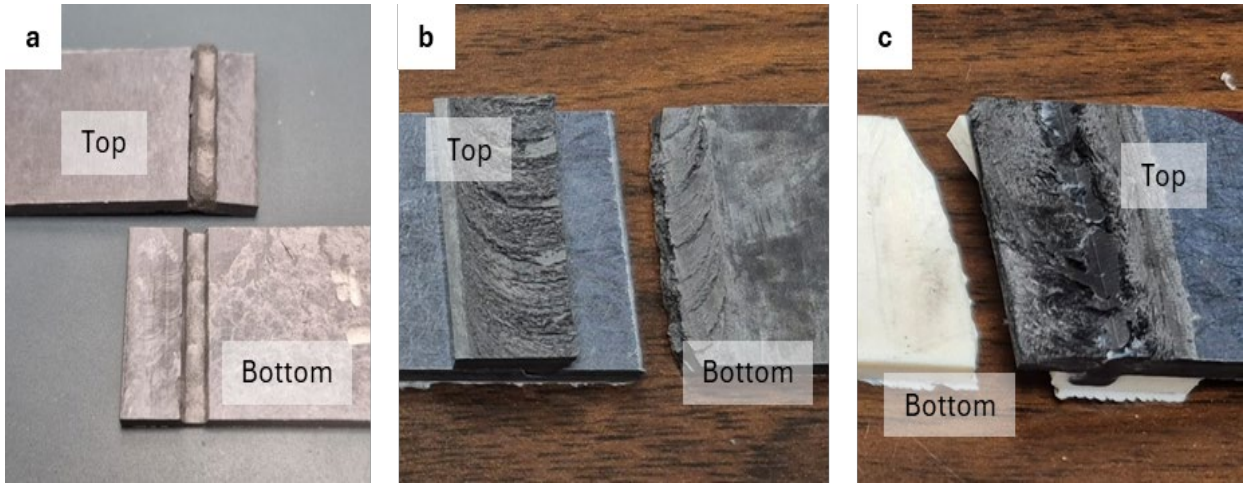

Fig. 4. Failure modes of samples 1 (a), 2 (b), and 7 (c) showing failure is dominated by tension in the weakest side of the sample.

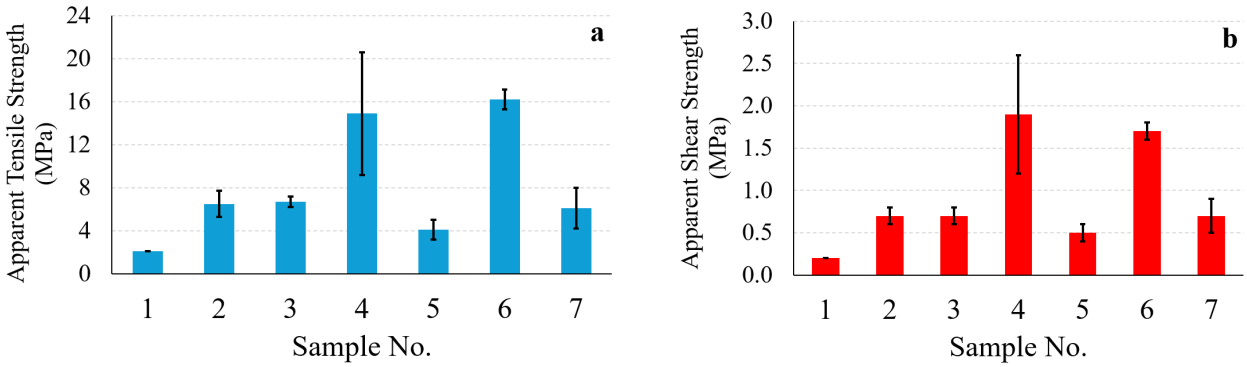

Fig. 5. Apparent (a) tensile and (b) lap shear strength graphs.

Differential Scanning Calorimetry (DSC).

DSC results indicate a slight decrease in crystallization and slight increase in the melting onset and peak temperatures in the weld area for most of the samples, as shown in Fig. 6. The standard deviation is represented by black error bars. The results indicate thermo-oxidative degradation, in which the PPS begins to crosslink, thereby impeding crystallization and increasing transition temperatures [21]. This degradation is most prevalent at temperatures well above the melting temperature of PPS in the presence of oxygen. While the temperature data acquired during FSW testing does not show such temperatures, the true temperature in the weld zone may be masked by the tool and surrounding sample. Given the welding occurred in standard atmosphere and optical microscopy results show evidence of melting, it is hypothesized that these small changes are attributed to thermo-oxidative degradation during welding.

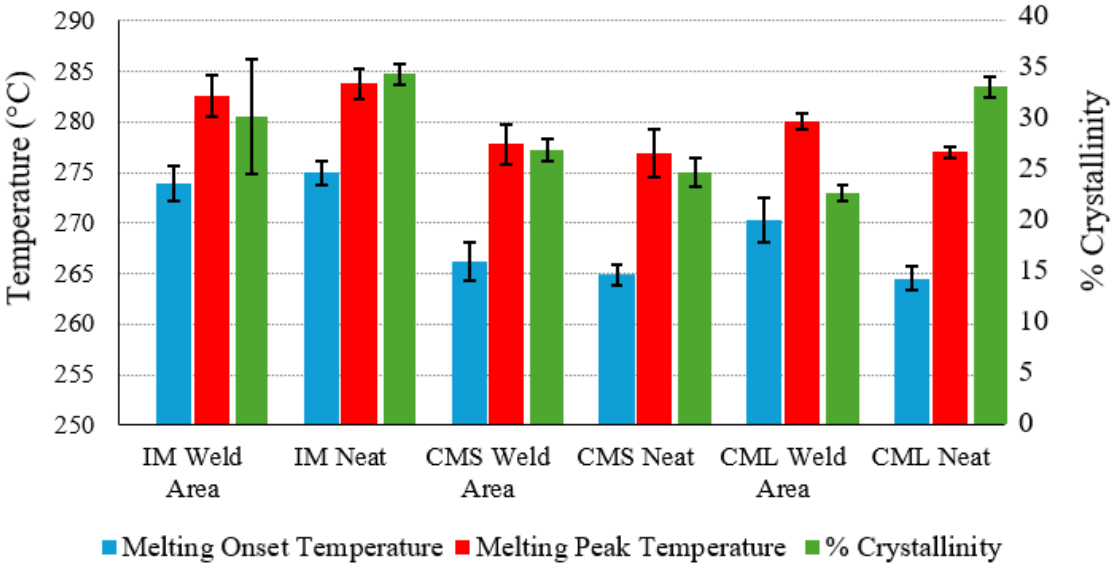

Fig. 6. DSC for welded & unwelded areas of each material.

Optical Microscopy (OM).

Transverse weld sections were observed by way of optical microscopy (OM) to analyze the interaction between fiber length and orientation in and around the weld zone. Fig. 7a shows sample 6, consisting of quasi-isotropic layers of continuous unidirectional carbon fiber, after welding. Outside of the weld zone, the laminate sequence is retained. Meanwhile, the stir zone (SZ) exhibits severe fiber disruption along with voids on both sides of the thermomechanically affected zone (TMAZ) and in the root of the weld. Sample 4 exhibited similar fiber disruption within the SZ as shown in Fig. 7b. Within the SZ, plastic deformation caused by the rotation and longitudinal motion of the tool likely damaged fibers as evident from lateral voids indicating fiber pull-out. It was observed that both fiber length and orientation were severely disrupted by the FSW process, with post-weld mechanical conditions relying heavily on the degraded polymer properties. Fig. 7c shows the transverse weld section of sample 7. Evidence of fiber migration within the weld can be seen from the top plate into the bottom plate. While not as clearly apparent in the other samples, due to difficulty in tracking fiber migration, this indicates that the bridging effect likely contributes to the differences in apparent lap strength for composites with longer fibers. The cross-sectional area of the weld zone was mostly constant for all composite base materials (ranging from 4.9 to 6.1 mm^2) but increased substantially when the base material did not contain reinforcing fibers (8.9 to 10.1 mm^2), indicating that fiber migration is strongly dependent on the material surrounding the SZ.

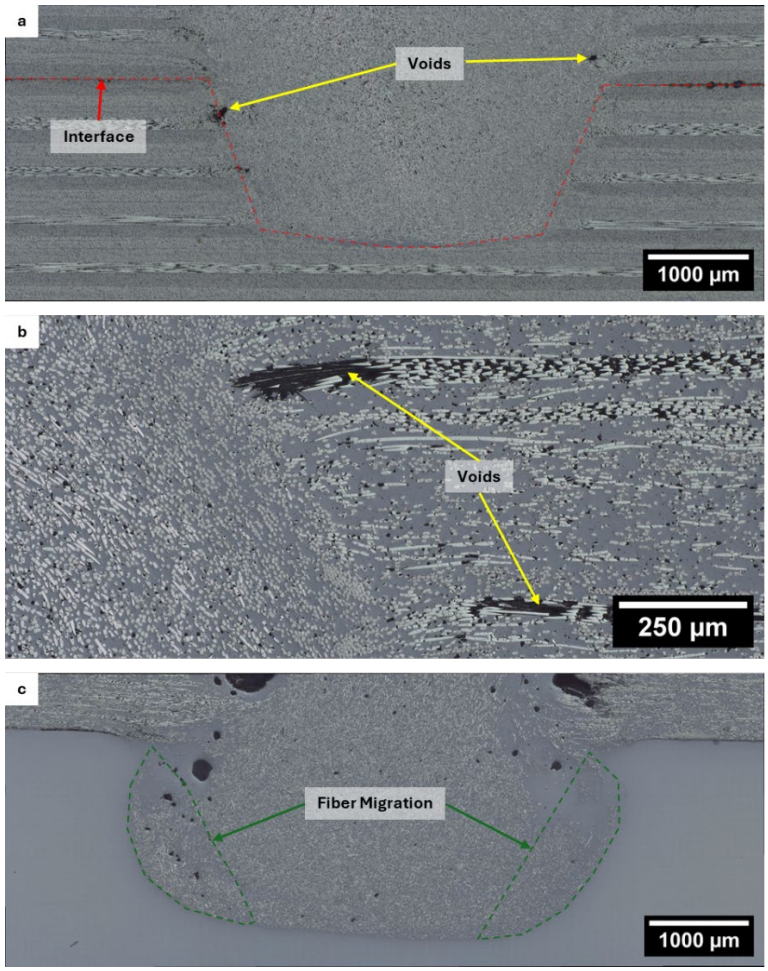

Fig. 7. Transverse section of samples 6 (a), 4 (b), and 7 (c) weld regions.

Surface Roughness.

Optical profilometry was utilized to measure the surface roughness. The results are listed in Table 6 along with the weld area. In general, samples with CMS on the weld side had higher S_z than IM samples, while CML welds showed the lowest peak-to-valley variation. The S_a results were generally more similar between materials, with the exception of samples 5 and 7, which also exhibited the largest S_q values. This is likely due to lower stiffness in the bottom plates resulting in greater fiber migration.

Table 6. Optical microscopy results.

Sample #	S_a (µm)	S_z (µm)	S_q (µm)	Weld area (mm^2)
1	135.6 ± 31.8	1157.8 ± 95.0	184.5 ± 25.0	-
2	139.9 ± 44.0	1155.9 ± 288.9	177.3 ± 52.9	5.655
3	98.4 ± 14.6	859.9 ± 233.2	127.5 ± 25.0	4.919
4	108.6 ± 36.7	1070.1 ± 112.5	147.1 ± 38.0	4.917
5	172.5 ± 67.2	1665.2 ± 701.5	240.0 ± 102.9	4.589
6	117.7 ± 12.5	840.5 ± 142.6	147.8 ± 19.7	5.378
7	272.2 ± 63.1	2260.2 ± 744.8	353.9 ± 80.2	9.459

Conclusion

In the current work, polyphenylene sulfide (PPS) with varying lengths of carbon fiber reinforcement were joined by FSW to measure the effect of fiber length on mechanical and microstructural properties. While fiber migration was observed by optical microscopy, the absence of characteristic shear failure and minimal fiber bridging does not inherently convey that fiber integrity was transferred through the bond line. There is evidence that continuous plastic deformation in the weld zone

diminished fiber length and orientation while the thermal input during welding caused polymer degradation, reducing mechanical strength within the weld zone. Although the apparent tensile and shear strength of the welded samples in this study was a fraction of the parent material, CF/PPS with longer fiber lengths did exhibit a positive relation to mechanical strength.
Key findings from this study include:

- Welding generally increased melting onset and peak temperature, indicating thermal degradation of the polymer matrix.
- The FSW process led to macrostructures dominated by mechanical interlocking rather than adhesive bonding.
- Severe fiber disruption and misorientation were present in the weld area, regardless of fiber length.
- A positive relationship between fiber length and weld strength was observed with fiber migration visible in the weld area, indicating some bridging effect.

Future Work

Future work will continue to focus on optimizing FSW parameters in pursuit of mechanical properties more closely aligned with the CF/PPS parent material.

Acknowledgement

The authors would like to thank Arame Cisse, Broc Dawson, Kristofer Laser Jr., Senudin Mehinovic, and Mason Sheeley along with Andrew and Christopher Bartlett of Penn State Behrend for their assistance with the experimental work. The authors would also like to thank Gen 2 Carbon for their donation of the recycled carbon fiber nonwoven used in this work. We acknowledge the partial support of the US National Science Foundation in the form of a Travel Support Grant [CMMI 2511050], which enabled the authors to attend and present at this conference.

References

[1] Ben Gur, H., & Banks-Sills, L. (2023). Evaluation of the effect of fiber bridging on mode I quasi-static testing. Fatigue & Fracture of Engineering Materials & Structures, 46(4), 1357–1374. https://doi.org/10.1111/ffe.13930.

[2] Fu, S. (1996). Effects of fiber length and fiber orientation distributions on the tensile strength of short-fiber-reinforced polymers. Composites Science and Technology, 56(10), 1179–1190. https://doi.org/10.1016/S0266-3538(96)00072-3.

[3] Barnett, P. R., Hmeidat, N. S., Zheng, B., & Penumadu, D. (2024). Toward a circular economy: Zero-waste manufacturing of carbon fiber-reinforced thermoplastic composites. Npj Materials Sustainability, 2(1), 3. https://doi.org/10.1038/s44296-024-00006-y.

[4] Wan, Y., & Takahashi, J. (2016). Tensile and compressive properties of chopped carbon fiber tapes reinforced thermoplastics with different fiber lengths and molding pressures. Composites Part A: Applied Science and Manufacturing, 87, 271–281. ttps://doi.org/10.1016/j.compositesa.2016.05.005.

[5] Barnett, P. R., Gilbert, C. L., & Penumadu, D. (2021). Repurposed/recycled discontinuous carbon fiber organosheet development and composite properties. Composites Part C: Open Access, 4, 100092. https://doi.org/10.1016/j.jcomc.2020.100092.

[6] Toray Advanced Composites. (2024, July 30). Toray Cetex TC1100 PPS. Product Data Sheet. https://www.toraytac.com/media/221a4fcf-6a4d-49f3-837f-9d85c3c34f74/dMki-Q/TAC/.

[7] Mitsubishi Chemical Advanced Materials. (2025, January 11). Techtron PSBG PPS. https://www.mcam.com/mam/54329/AEP-Techtron%E2%84%A2%20PSBG%20PPS_en_US.pdf.

[8] Toray Advanced Composites. (2019, July 12). Toray Cetex® MC1100 PPS. https://www.toraytac.com/media/f9d7ef67-9e40-47b8-addb-c82cbdd235aa.

[9] Akbari, M., Aliha, M. R. M., & Berto, F. (2023). Investigating the role of different components of friction stir welding tools on the generated heat and strain. Forces in Mechanics, 10, 100166. https://doi.org/10.1016/j.finmec.2023.100166.

[10] Neto, D. M., & Neto, P. (2013). Numerical modeling of friction stir welding process: A literature review. The International Journal of Advanced Manufacturing Technology, 65(1–4), 115–126. https://doi.org/10.1007/s00170-012-4154-8.

[11] Carbon (Xiamen) New Material Co., Ltd. (2024). Carbon Fiber Reinforced Polymers [Technical]. https://www.carbonele.com/pps-cf10-durable-polyphenylene-sulfide-carbon-fiber-lend/#0.

[12] Ahmed, H., Van Tooren, M., Justice, J., Harik, R., Kidane, A., & Reynolds, A. (2019). Investigation and development of friction stir welding process for unreinforced polyphenylene sulfide and reinforced polyetheretherketone. Journal of Thermoplastic Composite Materials, 32(9), 1242–1267. https://doi.org/10.1177/0892705718785676.

[13] Eslami, S., Tavares, P. J., & Moreira, P. M. G. P. (2017). Friction stir welding tooling for polymers: Review and prospects. The International Journal of Advanced Manufacturing Technology, 89(5–8), 1677–1690. https://doi.org/10.1007/s00170-016-9205-0.

[14] Yang, F., & Pitchumani, R. (2002). Healing of Thermoplastic Polymers at an Interface under Nonisothermal Conditions. Macromolecules, 35(8), 3213–3224. https://doi.org/10.1021/ma010858o.

[15] Ebert, C., Dürr, M. N., & Bonten, C. (2025). Functionalization of Continuous Fiber-Reinforced Thermoplastic Pultrusion Profiles by Welding. Journal of Composites Science, 9(1), 6. https://doi.org/10.3390/jcs9010006.

[16] ASTM International, 2025, “Standard Test Method for Tensile Properties of Polymer Matrix Composite Materials.” https://doi.org/10.1520/D3039_D3039M-17R25.

[17] ASTM International, 2022, “Standard Test Method for Tensile Properties of Plastics.” https://doi.org/10.1520/D0638-22.

[18] ASTM International, 2023, “Standard Test Method for Lap Shear Adhesion for Fiber Reinforced Plastic (FRP) Bonding." https://doi.org/10.1520/D5868-01R23.

[19] ASTM International, 2023, “Standard Test Methods for Determining the Izod Pendulum Impact Resistance of Plastics.” https://doi.org/10.1520/D0256-23.

[20] Schindelin, J., Arganda-Carreras, I., Frise, E., Kaynig, V., Longair, M., Pietzsch, T., … Cardona, A. (2012). Fiji: an open-source platform for biological-image analysis. Nature Methods, 9(7), 676–682. https://doi.org/10.1038/nmeth.2019.

[21] Zuo, P., Tcharkhtchi, A., Shirinbayan, M., Fitoussi, J., & Bakir, F. (2019). Overall Investigation of Poly (Phenylene Sulfide) from Synthesis and Process to Applications-A Review. Macromolecular Materials and Engineering, 304(5), 1800686. https://doi.org/10.1002/mame.201800686.